Asian Journal of Chemistry; Vol. 33, No. 11 (2021), 2817-2825

ASIAN JOURNAL OF CHEMISTRY

https://doi.org/10.14233/ajchem.2021.23422

Spectral and Structural Characterization of Metformin with Different Counter Anions: Comparative Analysis and DFT Calculations

MOHAMMED ALSAWAT[1], HAMDY S. EL-SHESHTAWY[2], TARIQ ALTALHI[1], AMINE MEZNI[1], TUSHAR KUMERIA[3], SALIH S. AL-JUAID[4] and MOHAMED M. IBRAHIM[1,*]

[1]Department of Chemistry, Faculty of Science, Taif University, Taif, P. O. Box 11099, Taif 21944, Saudi Arabia
[2]Department of Chemistry, Faculty of Science, Kafrelsheikh University, Kafr El-Sheikh, Egypt
[3]School of Materials Science and Engineering, The University of New South Wales, Sydney, New South Wales, 2052, Australia
[4]Department of Chemistry, Faculty of Science, King Abdulaziz University, Jeddah, Saudi Arabia

*Corresponding author: E-mail: ibrahim@tu.edu.sa

Received: 19 July 2021; *Accepted*: 13 September 2021; *Published online*: 20 October 2021; AJC-20569

The metformin perchlorate ($MetH^+ \cdot ClO_4^-$) with a new crystal structure was synthesized, characterized and comparatively studied with other metformin salts of Cl^- and NO_3^- by different spectroscopic techniques such as TGA-DSC and FT-IR as well as UV-visible spectroscopic studies. DFT calculations were performed by rwb97xd and 6-31G+(d,p) basis set for structure optimization and frequency calculations. Similar to $MetH^+ \cdot Cl^-$, the crystal packing of $MetH^+ \cdot ClO_4^-$ and $MetH^+ \cdot NO_3^-$ were stabilized by hexagonal hydrogen bond elongated network. The relative stability and reactivity of these salts were determined by exploring the DFT chemical descriptors such as chemical hardness, electronegativity, electronic chemical potential, electrophilicity and hardness. These calculations were employed to get the subset of variables that could categorize the metformin salts according to their reactivity.

Keywords: Metformin, Spectroscopic studies, Reactivity descriptors, Density functional theory.

INTRODUCTION

Biguanides have been known as active molecules of building blocks in pharmaceutical drugs [1-3] and crystal engineering [4-6]. The unique physical and chemical properties of biguanides such as different donor and acceptor sites, as well as simple preparation and functionalization methods nominated the biguanide derivatives to be used in different applications. Metformin is a type-2 diabetes potent drug and recently known as anticancer [7-10] as well as anti-thyroid agents [11-14]. The crystal structure of metformin has been extensively investigated with different anions such as nitrate [15,16], chloride [17,18], bromide [19], acetate [20], carbamate [21], carbonate [22] and nitrate-perchlorate [23]. However, the crystal structure of metformin salt with perchlorate as a counter anion ($MetH^+ \cdot ClO_4^-$) has not been yet reported.

The crystal structures of metformin salts with different anions show different morphologies and spectroscopic properties. For example, in metformin hydrobromide ($MetH^+ \cdot Br^-$) [19] and metformin ethyl *N*-(3-tossulfonyl)carbamate [21], the position of the two -NH_2 groups were in the opposite direction. In contrast, the metastable metformin hydrochloride ($MetH^+ \cdot Cl^-$) [17,18] and metformin nitrate ($MetH^+ \cdot NO_3^-$) structures shows that the two -NH_2 groups are in the same direction. In case of the *cis*-NH_2 groups, the crystal packing of metformin salts shows hexagonal hydrogen bonding network [24].

Intermolecular forces have a significant involvement in helping to understand the interaction between atoms in the same or a different type of molecule. The interaction can include both polar or nonpolar molecules and ions. The proper orientation of the dipole moment could totally change the stability behaviour of the system. Consequently, the exchange of a single atom within the molecule causing the change of dipole moment orientation might be crucial for controlling the structural properties and intermolecular charge transfer. Therefore the computational techniques, which enable precise parameterization of these interactions, is very important [25].

The crystal structure of $MetH^+ \cdot ClO_4^-$ was synthesized and fully characterized. Its structure of $MetH^+ \cdot ClO_4^-$ was compared

with the analogue salts such as $MetH^+ \cdot Cl^-$, and $MetH^+ \cdot NO_3^-$ by different spectroscopic techniques such as FTIR, TGA-DSC, UV-visible spectroscopy. The main purpose of this study was the determination of chemical reactivity and sites selective of the metformin salts with ClO_4^-, Cl^- and NO_3^- as counter anions. Molecular geometries have been studied using the density functional theory (DFT) with rwb97xd and 6-31G+(d,p) basis set for structure optimization and frequency calculations. DFT chemical reactivity descriptors (chemical hardness, chemical potential, electronegativity, electrophilicity and softness) were also calculated for the three salts and used to predict their relative stability and reactivity.

EXPERIMENTAL

Metformin hydrochloride was purchased from Sigma-Aldrich, Germany. Single crystals of metformin nitrate and perchlorate were obtained by slow evaporation of aqueous solution of metformin acidified by conc. nitric acid and perchloric acid. Infrared was recorded with Alpha-Atunated FT-IR, Bruker from 4000 to 400 cm^{-1}. The crystallographic data (Table-1) were collected on a Smart CCD diffractometer of Bruker AXS using Mo$K\alpha$ radiation. Lorentz-Polarization and absorption corrections were performed by SAINT and SADABS programs [26,27]. The structures were solved by direct or Patterson methods using SHELXS-97 [28]. Thermal analyses were recorded on Shimadzu DTG 60H with system interface device in the atmosphere of nitrogen. Absorption spectra of metformin salts were measured by Cary Series UV-Vis-NIR spectrophotometer.

Computational details: The structures geometries were performed using Gaussian09 program [29]. The rwb97xd level was used in order to account for the weak interactions and dispersion forces and 6-31G+(d,p) basis set. The frequency calculations were performed on the optimized structure to confirm that the structures are minimum energy on the potential energy and calculate the theoretical IR frequencies. TD-DFT were used to simulate the absorption spectra of the salts.

TABLE–1
CRYSTAL DATA AND STRUCTURE REFINEMENT OF $MetH^+ \cdot NO_3^-$ AND $MetH^+ \cdot ClO_4^-$ SALTS

	$MetH^+ \cdot NO_3^-$	$MetH^+ \cdot ClO_4^-$
Empirical formula	$C_4H_{12}N_6O_3$	$C_4H_{12}N_5O_4Cl$
Formula weight	192.20	229.64
Temperature (K)	100(2)	100(2)
Wavelength (Å)	0.71073	0.71073
Crystal system	Triclinic	Monoclinic
Crystal habit	Translucent colorless block	Translucent colorless block
Crystal size (mm)	0.200 × 0.500 × 0.900	0.100 × 0.200 × 0.400
Space group	P –1	P 1 21/n 1
Z	2	4
Volume ($Å^3$)	4174.8(5)	965.89(7)
a (Å)	7.1676(11)	10.7268(4)
b (Å)	7.5368(12)	7.3049(3)
c (Å)	8.7968(14)	12.3941(5)
α (°)	78.167(3)	90
β (°)	73.793(3)	95.9850(10)
γ (°)	85.511(4)	90
Density (calc.) (g/cm^3)	1.430	1.579
Absorption coefficient (mm^{-1})	0.120	0.397
F(000)	204	480
θ-range (°)	2.46 to 28.32	2.39 to 28.32
Index ranges	–9<=h<=9; –10<=k<=10; –11<=l<=11	–14<=h<=14; –9<=k<=9; –16<=l<=16
Refinement method	Full–matrix least–squares on F2	Full–matrix least–squares on F2
Refinement program	SHELXL–2014 (Sheldrick, 2014)	SHELXL–2014 (Sheldrick, 2014)
Function minimized	$\Sigma w(F_o^2 - F_c^2)^2$	
Reflections collected	8121	8959
Independent reflections	2200 [R(int) = 0.0104]	2388 [R(int) = 0.0111]
Max. and min. transmission	0.9760 and 0.8990	0.9610 and 0.8570
Data /restraints/parameters	2200/0/144	2388/0/153
Goodness–of–fit on F^2	1.055	1.076
Final R indices	2087 data; I > 2σ(I), R1 = 0.0299, wR2 = 0.0815, wR2 = 0.1323	2230 data; I > 2σ(I), R1 = 0.0252, wR2 = 0.0689
R indices (all data)	R1 = 0.0313, wR2 = 0.0832	R1 = 0.0272, wR2 = 0.0709
Weighting scheme	$w = 1/[\sigma^2(F_o^2) + (0.0434P)^2 + 0.1431P]$ where $P = (F_o^2 + 2F_c^2)/3$	$w = 1/[\sigma^2(F_o^2) + (0.0380P)^2 + 0.4265P]$ where $P = (F_o^2 + 2F_c^2)/3$
Largest diff. peak (e. $Å^{-3}$) and hole	0.259 and –0.263	0.301 and –0.491
R.M.S. deviation from mean (e $Å^{-3}$)	0.043	0.050

Chemical descriptors such as global hardness (η) of the compounds was calculated by eqn. 1:

$$\eta = \frac{E_{HOMO} - E_{LUMO}}{2} \quad (1)$$

The electronic chemical potential was calculated by eqn. 2:

$$\mu = \frac{E_{HOMO} + E_{LUMO}}{2} \quad (2)$$

The electronegativity (χ) of the molecules was calculated from $\chi = -\mu$, where the electronegativity index (ω) was calculated by eqn. 3:

$$\omega = \frac{\mu^2}{2\eta} \quad (3)$$

The softness of the molecules was calculated by eqn. 4:

$$S = \frac{1}{2\eta} \quad (4)$$

RESULTS AND DISCUSSION

Metformin salts of nitrate ($MetH^+ \cdot NO_3^-$) and perchlorate ($MetH^+ \cdot ClO_4^-$) have been determined by single crystal X-ray diffraction. Figs. 1a and 2a illustrate the ORTEP drawing of $MetH^+ \cdot NO_3^-$ and $MetH^+ \cdot ClO_4^-$ with thermal ellipsoids of 50% probability level. Their bond lengths and angles are listed in Tables 2 and 3. The inter- and intramolecular hydrogen bonding arrangements are displayed in Figs. 1b and 2b. The average C-N bond distances of 1.376(11) and 1.388(10) Å in $MetH^+ \cdot NO_3^-$ and $MetH^+ \cdot ClO_4^-$, respectively are higher than those found in C=N bond distances, which indicates the delocalization of the π-electrons over the –C=N-C=N-skeleton. In addition, the bond distances in $MetH^+ \cdot ClO_4^-$ are higher than the reported values for $(MetH)_2^{2+} \cdot NO_3^- \cdot ClO_4^-$ salt [23] and then those found in $MetH^+ \cdot Cl^-$, which has average C-N bond distances of 1.336(4) Å [17]. Also, the N-C-N bond angles vary from 118.66(8)° to 124.10(8)° in $MetH^+ \cdot NO_3^-$ and from 117.46(9)° to 124.81(9)° in $MetH^+ \cdot ClO_4^-$. These bond angles are slightly higher than those found in $MetH^+ \cdot Cl^-$. Similar to $MetH^+ \cdot Cl^-$, the imino group attached to C3 in $MetH^+ \cdot NO_3^-$ and C2 in $MetH^+ \cdot ClO_4^-$ are protonated whereas in iother biguanide salts, the protonation occurs at the terminal imino group [30]. Both $MetH^+ \cdot NO_3^-$ and $MetH^+ \cdot ClO_4^-$ structures show that the N3 is not protonated, which was in agreement with literature [24]. The orientation of the two NH_2 groups on the same side in $MetH^+ \cdot ClO_4^-$ was in accordance with the most stable metastable reported form of $MetH^+ \cdot NO_3^-$ [16] and $MetH^+ \cdot Cl^-$ [18]. The crystal packing of $MetH^+ \cdot ClO_4^-$ and $MetH^+ \cdot NO_3^-$ are stabilized by the hexagonal hydrogen bond network through the N2H…N3 and N5H…N3 (Figs. 1b and 2b). The molecules in the unit cell are stabilized by N…H….O and N…H….Cl types of hydrogen bond, which are located around the centers of inversion as seen in the packing diagram (Fig. 1c and 2c).

FT-IR spectra of the three metformin salts are shown in Fig. 3. The stretching vibration peaks, assigned to symmetric and asymmetric N-H stretching vibrations, respectively have been appeared in the range of 3447-3300 and 3176-3112 cm^{-1}. The N-H deformation vibrations occur in the region of 1626-1564 cm^{-1}. Weak intensity bands appearing in the frequency range 1275-1061 cm^{-1} have been assigned to the C-N stretching vibrations. The weak bands at 800, 843 and 783 cm^{-1} have been assigned to NH_2 rocking vibrations of $MetH^+ \cdot Cl^-$, $MetH^+ \cdot NO_3^-$ and $MetH^+ \cdot ClO_4^-$, respectively.

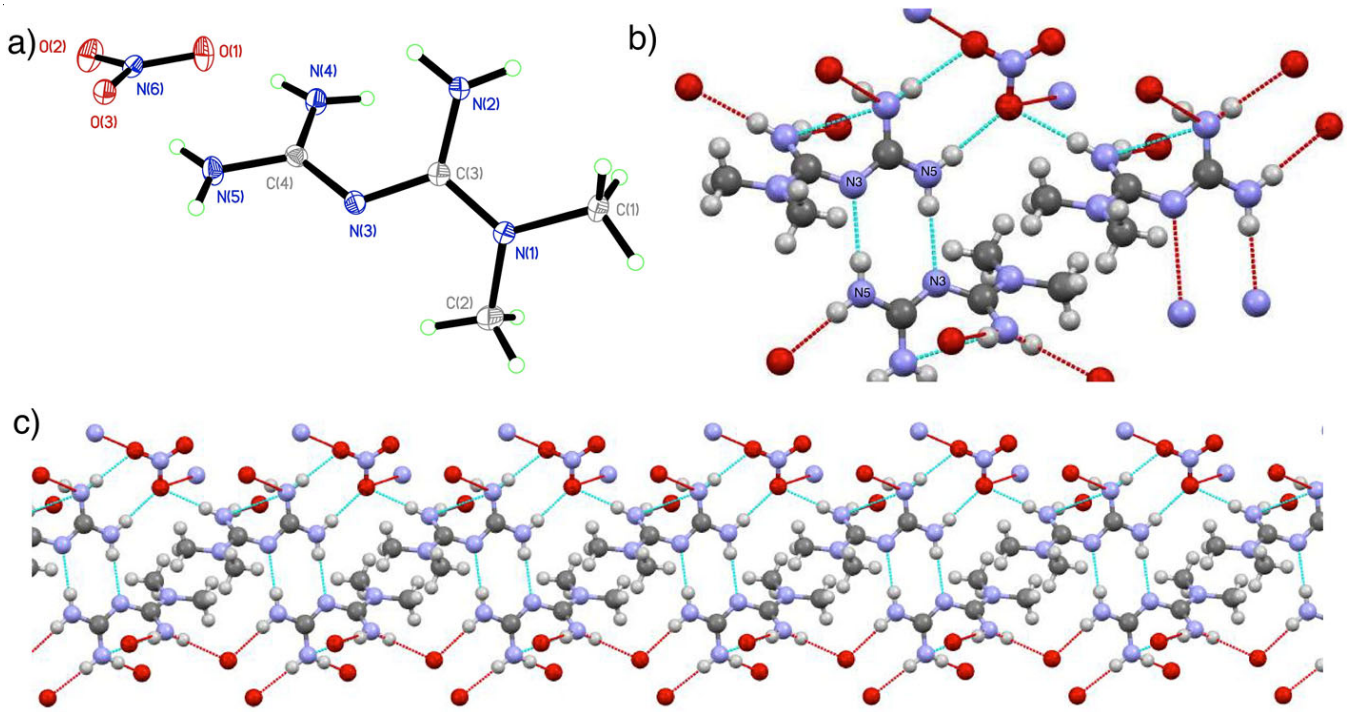

Fig. 1. Molecular structure of $Met^+ \cdot NO_3^-$ (a) ORTEP drawing with thermal ellipsoids of 50% probability level; (b) hexagonal hydrogen bond network (c) Projection along *c* axis, describing the geometry in the ribbons which are formed from $Met^+ \cdot NO_3^-$ inter and intra hydrogen bonding displaye

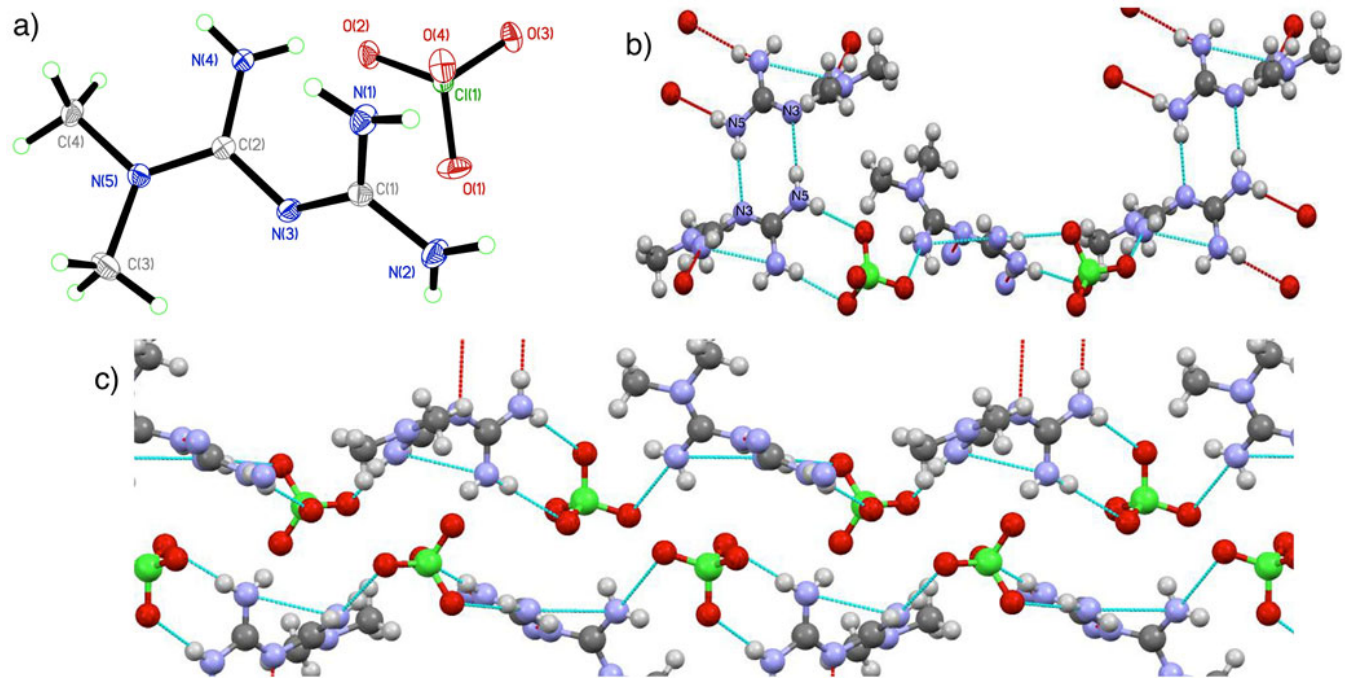

Fig. 2. Molecular structure of $Met^{+}\cdot ClO_4^{-}$ (a) ORTEP drawing with thermal ellipsoids of 50% probability level; (b) hexagonal hydrogen bond network (c) Projection along *c* axis, describing the geometry in the ribbons which are formed from $Met^{+}\cdot ClO_4^{-}$ inter and intra hydrogen bonding displayed

TABLE-2
SELECTED BOND LENGTHS (Å), BOND ANGLES (°), AND HYDROGEN BOND GEOMETRY OF $MetH^{+}\cdot NO_3^{-}$

Bond lengths (Å) and bond angles (°)							
C1–N1	1.4616(11)	N6–O3	1.2768(9)	N2–C3–N3	122.27(7)	N1–C3–N3	118.69(7)
C2–N1	1.4616(11)	C3–N2	1.3412(11)	N5–C4–N4	117.89(8)	N5–C4–N3	117.93(7)
C3–N1	1.3372(10)	C4–N5	1.3332(11)	C3–N1–C2	121.51(7)	N3–C4–N4	124.10(8)
C3–N3	1.3495(11)	C4–N4	1.3429(11)	C2–N1–C1	117.03(7)	C3–N1–C1	120.71(7)
C4–N3	1.3377(11)	N6–O1	1.2533(10)	O2–N6–O3	119.49(7)	O1–N6–O3	119.02(7)
N6–O2	1.2334(10)	N1–C3–N2	118.66(8)	N1–C3–N2	118.66(8)		

Hydrogen bond lengths (Å) and bond angles (°)				
D–H···A	D(D–H)	d(H···A)	d(D···A)	∠(DHA)
C1–H1A···O2	0.98	2.43	3.2975(11)	147.4
C1–H1B···O2	0.98	2.4	3.3713(12)	171.6
N4–H4A···O1	0.876(14)	2.133(14)	2.9423(11)	153.4(12)
N4–H5A···O1	0.862(15)	2.089(15)	2.9334(11)	166.1(13)
N5–H6A···N3	0.871(14)	2.127(14)	2.9952(11)	174.5(13)
N2–H7A···O3	0.869(14)	2.142(14)	2.9983(10)	168.4(12)
N5–H7A···O3	0.864(14)	2.084(14)	2.9461(10)	175.1(12)
N2–H8A···O3	0.871(14)	2.123(14)	2.9662(11)	162.9(12)

Symmetry transformations used to generate equivalent atoms #1 –x+1, –y, –z+1; #2 x+1/2, –y+1/2, z–1/2

The methyl group vibrations appeared in the range of 2942-2298 cm^{-1}. These groups were found to be unaffected by other functional groups present in the molecule. Medium to strong absorption bands appeared in the range of 580-498 cm^{-1} are due to the C-N-C deformation. Strong vibration bands were observed at 1340 and 1102 cm^{-1}, assigned to the NO_3^{-} and ClO_4^{-} anions of the $MetH^{+}.NO_3^{-}$, and $MetH^{+}.ClO_4$ respectively. Simulated vibration frequencies of metformin salts is shown in Fig. 4. The stretching vibrations of N-H group were located at 3390, 3378, and 3365 for $MetH^{+}\cdot Cl^{-}$, $MetH^{+}\cdot NO_3^{-}$ and $MetH^{+}\cdot ClO_4^{-}$, respectively. The aliphatic C-H groups show frequency peaks in 2800-2500 cm^{-1} region (Table-4).

Figs. 5 and 6 show the TGA-DSC curves of $MetH^{+}\cdot NO_3^{-}$, and $MetH^{+}\cdot ClO_4^{-}$. Fig. 5 shows an endothermic peak at 226 ºC with no weight loss observed, indicating the probability of melting of $MetH^{+}\cdot NO_3^{-}$ at this temperature. This was in consistence with the melting of $MetH^{+}\cdot Cl^{-}$, which showed an endothermic peak at 229.89 ºC [31,32]. Whereas the melting of $MetH^{+}\cdot ClO_4^{-}$ started with exothermic peak at 134 ºC (Fig. 6). The thermal decomposition of both salts occurs in five weight loss steps. The first weight loss steps with endothermic peaks of 11.31% at 325.6 ºC and 11.22% at 321.7 ºC may be attributed to the removal of NH_3 molecule from $MetH^{+}\cdot NO_3^{-}$ and $MetH^{+}\cdot ClO_4^{-}$, respectively. The release of NH_3 leads to the formation

TABLE-3
SELECTED BOND LENGTHS (Å), BOND ANGLES (°) AND HYDROGEN BOND GEOMETRY OF $MetH^+ \cdot ClO_4^-$

Bond lengths (Å) and bond angles (°)							
C1–N3	1.3317(13)	C2–N3	1.3517(13)	N5–C2–N3	118.99(9)	N5–C2–N4	118.85(9)
C1–N1	1.3475(13)	Cl1–O1	1.4344(8)	O1–Cl1–O2	110.64(5)	N4–C2–N3	121.88(9)
C2–N4	1.3399(13)	Cl1–O4	1.4484(8)	O2–Cl1–O4	109.70(5)	O1–Cl1–O4	110.22(5)
C3–N5	1.4627(13)	Cl1–O2	1.4350(8)	O2–Cl1–O3	109.10(5)	O1–Cl1–O3	108.96(5)
C4–N5	1.4617(13)	Cl1–O3	1.4620(8)	C2–N5–C4	120.54(8)	O4–Cl1–O3	108.17(5)
C1–N2	1.3370(13)	N3–C1–N2	117.46(9)	C4–N5–C3	116.82(8)	C2–N5–C3	121.30(9)
C2–N5	1.3334(13)	N2–C1–N1	117.68(9)	N3–C1–N1	124.81(9)		

Hydrogen bond lengths (Å) and bond angles (°)				
D–H···A	D(D–H)	d(H···A)	d(D···A)	∠(DHA)
C4–H4B···O2	0.98	2.56	3.2910(13)	131.5
N1–H1A···Cl1	0.843(16)	2.962(17)	3.7811(10)	164.6(15)
N1–H1A···O4	0.843(16)	2.215(17)	3.0423(12)	166.9(16)
N2–H2A···O3	0.842(17)	2.204(17)	3.0421(12)	173.1(16)
N1–H1B···N4	0.810(19)	2.524(17)	2.9063(13)	110.3(14)
N1–H1B···O1	0.810(19)	2.539(19)	3.2156(14)	141.9(15)
N1–H1B···O3	0.810(19)	2.539(19)	3.3004(13)	157.2(15)
N2–H2B···N3	0.860(16)	2.159(16)	3.0184(13)	177.3(14)
N4–H4D···Cl1	0.802(17)	2.924(16)	3.5050(9)	131.2(13)
N4–H4D···O3	0.802(17)	2.344(16)	3.1123(12)	160.9(15)
N4–H4E···O4	0.812(16)	2.329(16)	3.0841(12)	155.0(13)

Symmetry transformations used to generate equivalent atoms #1 –x+1, –y, –z+1; #2 x+1/2, –y+1/2, z–1/2

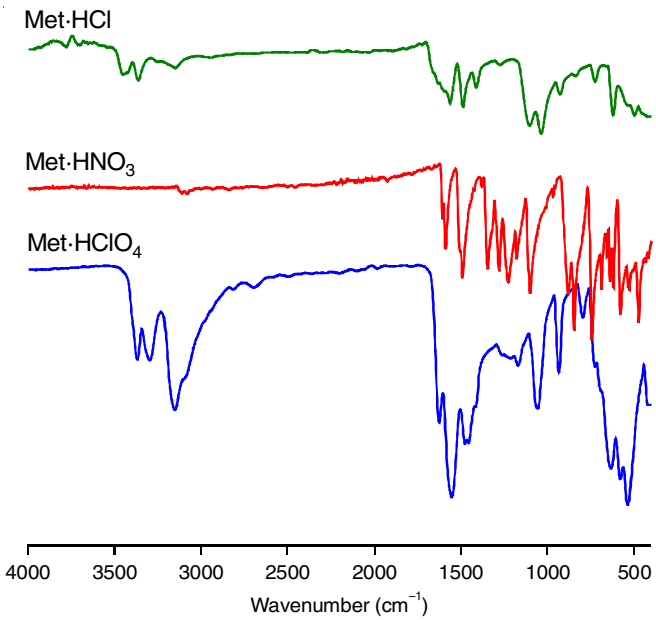

Fig. 3. Experimental FT-IR spectra of the metformin salts $MetH^+ \cdot Cl^-$, $MetH^+ \cdot NO_3^-$ and $MetH^+ \cdot ClO_4^-$

unstable intermediate adducts $C_4H_9N_5O_3$ and $C_4H_9ClN_4O_4$, respectively. In case of $MetH^+ \cdot NO_3^-$ and additional heating results in a second weight loss of 36.11% with an exothermic peak at 403.7 ºC. This could be assignable to the elimination of one molecule of HNO_3. In case of $MetH^+ \cdot ClO_4^-$, the second step was accompanied by an endothermic peak at 337.2 ºC with a weight loss of 57.42%. This may be assignable to the elimination of one $HClO_4$ molecule . The third, fourth, and fifth steps in both salts were difficult to be distinguished. These steps may be related to the decomposition of the remaining organics in both salts such as ethylene, dicyanamide, HCN and N_2, leaving carbon as a residue [32].

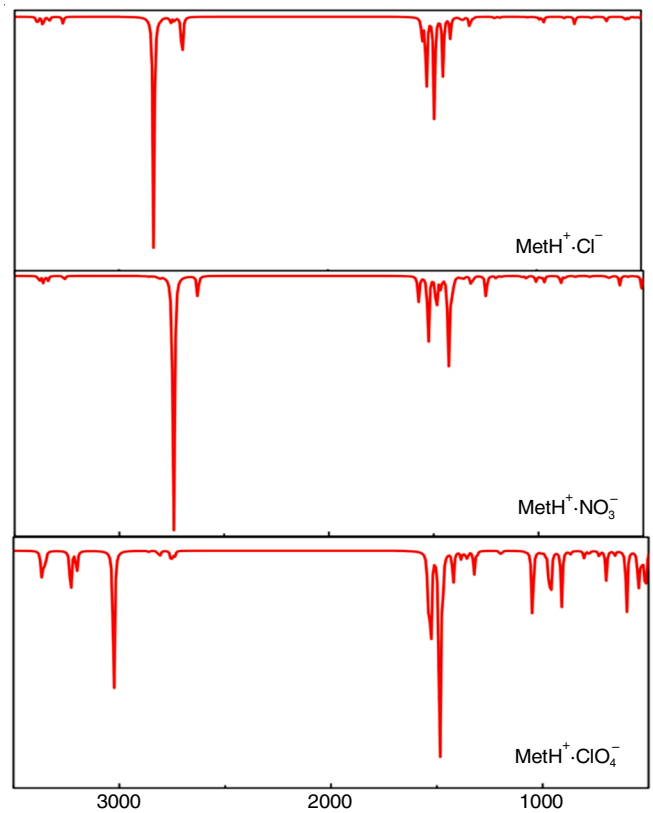

Fig. 4. Simulated frequency vibrations of $MetH^+ \cdot Cl^-$, $MetH^+ \cdot NO_3^-$ and $MetH^+ \cdot ClO_4^-$ at rwb97xd/6-31+g(d,p) in the gas phase (data were scaled by 1.0)

Experimental and simulated UV-Vis spectroscopy: The calculated frontiers orbitals of $MetH^+ \cdot Cl^-$, $MetH^+ \cdot NO_3^-$ and $MetH^+ \cdot ClO_4^-$ are shown in Table-5. In $MetH^+ \cdot Cl^-$ and $MetH^+ \cdot NO_3^-$, the HOMO orbitals are located on the counter anion. Whereas in $MetH^+ \cdot ClO_4^-$, the HOMO orbitals are distributed

TABLE-4
EXPERIMENTAL, CALCULATED AND PEAK ASSIGNMENTS OF FTIR FOR $MetH^+\cdot Cl^-$, $MetH^+\cdot NO_3^-$ AND $MetH^+\cdot ClO_4^-$ SALTS

$MetH^+\cdot Cl^-$	$MetH^+\cdot NO_3^-$	$MetH^+\cdot ClO_4^-$	Assignments
3372 (sm), (3390)[a]	–, (3378)[a]	3447 (m), (3365)[a]	N–H stretching
3300 (m), (3336), 3176 (m), (3330)	(3360), 3112 (mw)	3362 (m), (3228), 3150 (w)	Asymmetric N–H stretching
2816 (w), (2830), 2619 (vw), (2690)	2801 (w), (2740), 2298 vw, (2630)	2942 (vw), (3002), 2302 (vw)	$(CH_3)_2N$ absorption
1626 (s), (1550)	1590 (w), (1580)	1564 (s), (1530)	N–H deformation
1475 (sm), (1486)	1494 (mw), (1480)	1487 (s), (1480)	Symmetric N–H deformation
–	1340 (s), (1325)	–	NO_3^-
1170 (w), (1170), 1061 (mw)	1227 (w), (1245), 1098 (w)	1275 (vs), (1301)	C–N stretching
–	–	1102 (vs), (1048), 1037 (vs)	ClO_4^-
936 (mw)	880 (s), (887)	928, (960)	N–H out of plane bending
800 (w), (815)	843 (w)	784, (801)	NH_2 rocking
736 (mw)	739 (w), (600)	726, (735)	N–H wagging
633 (m) 524, (650)	626 (w)	621, (600)	C–H out of plane bending
580 (m)	526 (m)	498, (540)	C–N–C deformation

[a]Values in brackets are the calculated frequency at rwb97xd/6–31+g(d,p) level

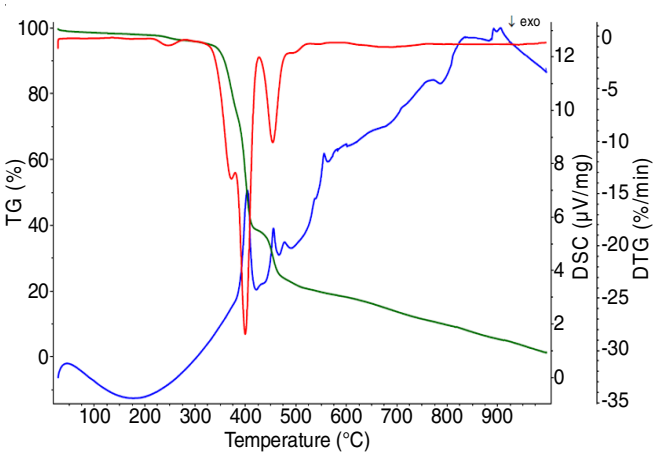

Fig. 5. TGA-DTG-DSC curves of $Met^+\cdot NO_3^-$

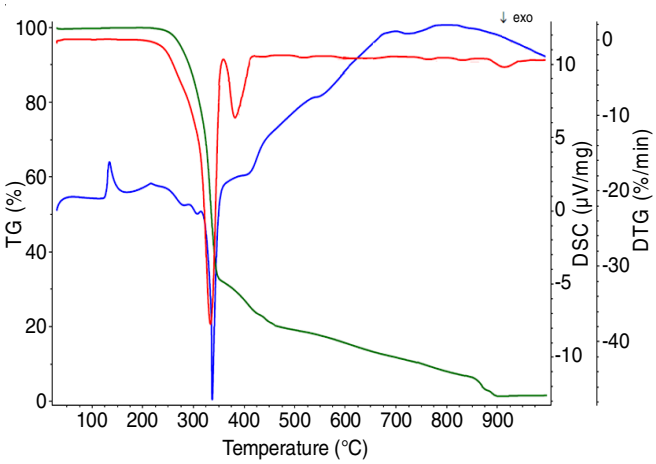

Fig. 6. TGA-DTG-DSC curves of $Met^+\cdot ClO_4^-$

over the whole molecule. On the other hand, the LUMO orbitals are located over the $MetH^+$ moiety for all salts. The calculated energy gap (E_g) shows that $MetH^+\cdot ClO_4^-$ is more stable than those found in $MetH^+\cdot Cl^-$ and $MetH^+\cdot NO_3^-$ salts, as the former has high E_g value.

The UV-visible absorption spectra of $MetH^+\cdot Cl^-$, $MetH^+\cdot NO_3^-$ and $MetH^+\cdot ClO_4^-$ were measured in aqueous solution (Fig. 7a). The electronic spectra show the presence of peaks at 234, 233 and 235 nm for $MetH^+\cdot Cl^-$, $MetH^+\cdot NO_3^-$ and $MetH^+\cdot ClO_4^-$, respectively, which may be ascribed to the –C=N-C=N- skeleton [33]. The calculated absorption peaks (TD-DFT) were found to be 230, 235 and 238 nm for $MetH^+\cdot Cl^-$, $MetH^+\cdot NO_3^-$ and $MetH^+\cdot ClO_4^-$, respectively (Fig. 7b). In addition, the electronic spectrum of $MetH^+\cdot ClO_4^-$ in the vacuum UV region shows the presence of an extra peak at 209 nm. This corresponds to the experimental peak, which appeared at 205 nm. The presence of the two peaks in $MetH^+\cdot ClO_4^-$, were ascribed to the presence equilibrium of conjugated (isomer I, -C=N-C=N-) and unconjugated (isomer II, =C-NH-C-N=) forms [33]. The presence of the unconjugated form suggests that protonation could occur at the terminal N atom as well as the N2 position in $MetH^+\cdot ClO_4^-$. In contrast to the $MetH^+\cdot Cl^-$ and $MetH^+\cdot NO_3^-$ salts, the isomer I is more stable than isomer (II) by 2.7 kcal/mol.

The molecular electrostatic surface potential (MESP) technique has been widely used to explore the molecular reactivity of molecules [34,35]. The negative electrostatic potentials are prone to electrophilic attach, where the positive electrostatic potentials are subjected to nucleophilic attack. In biological systems, the MESP are used for binding site recognition. In order to predict the reactive binding sites of different metformin salts, MESP were calculated at rwb97xd/6-31G+(d,p) level in the gas phase. Fig. 8 shows that the negative reactive sites are located on the counter anion moieties, which nominated for the electrophilic attack. Whereas the positive sites are located on protonated metformin. The positive MESP on the protonated sites values were found to be +35.4, +25.1, and +21.2 for $MetH^+\cdot NO_3^-$, $MetH^+\cdot Cl^-$, and $MetH^+\cdot ClO_4^-$, respectively, predicting the strength of the compounds for nucleophilic attach in the same order.

The atomic charge transfer of $MetH^+\cdot Cl^-$, $MetH^+\cdot NO_3^-$ and $MetH^+\cdot ClO_4^-$ were calculated by Hirshfeld and Mullikan atomic charge analysis. Table-6 shows the calculated atomic charges from the optimized structures at rwb97xd/6-31G+(d,p) level of theory in the gas phase. The positive charge on the metformin salts are increasing in the order of $MetH^+\cdot Cl^- < MetH^+\cdot NO_3^- < MetH^+\cdot ClO_4^-$. The calculated dipole moment shows that $MetH^+\cdot NO_3^-$ has the largest dipole moment, which indicates higher tendency for intermolecular interaction [36].

TABLE-5
CALCULATED HOMO AND LUMO ORBITALS OF METFORMIN SALTS

	HOMO	LUMO
$MetH^+ \cdot Cl^-$	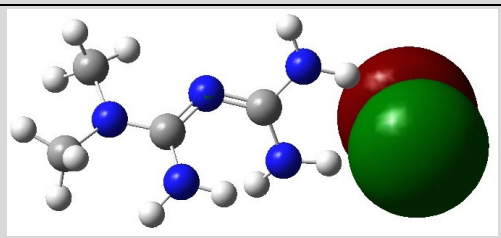	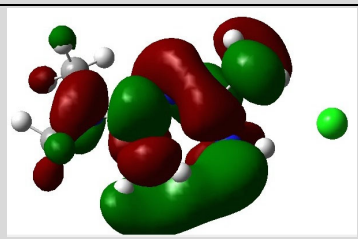
$MetH^+ \cdot NO_3^-$	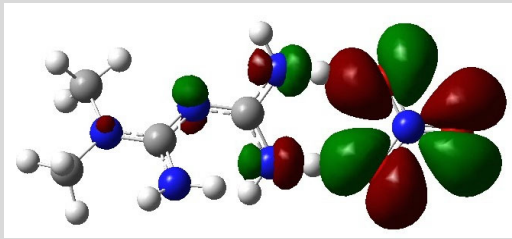	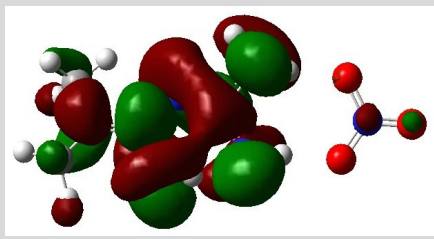
$MetH^+ \cdot ClO_4^-$	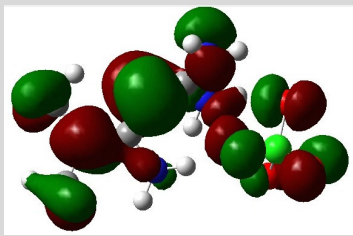	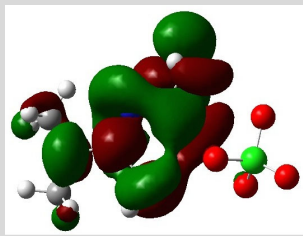

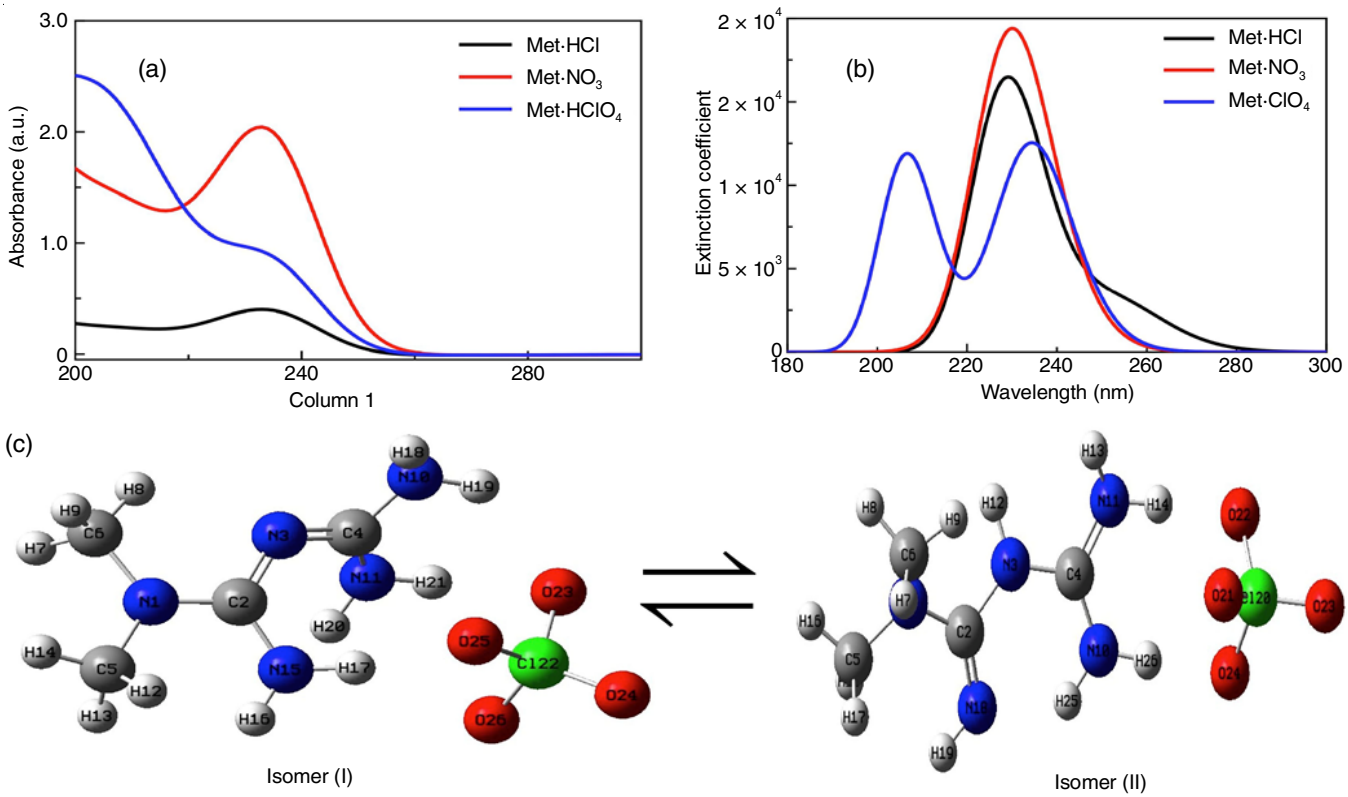

Fig. 7. (a) Experimental absorption spectra of metformin counter ions in aqueous solution, (b) simulated absorption spectra of metformin counter ions in water at rwb97xd/6-31+g(d,p) level of theory, (c) equilibrium between isomer (I) and (II)

DFT chemical reactivity descriptors {chemical hardness (η), chemical potential (μ), electronegativity (χ), electrophilicity (ω) and softness (S)} were calculated (Table-7). The chemical hardness of molecules are related to its chemical stability [37]. The $MetH^+ \cdot Cl^-$ with lower chemical hardness value indicates lower stability, which is suspected to be chemically changed.

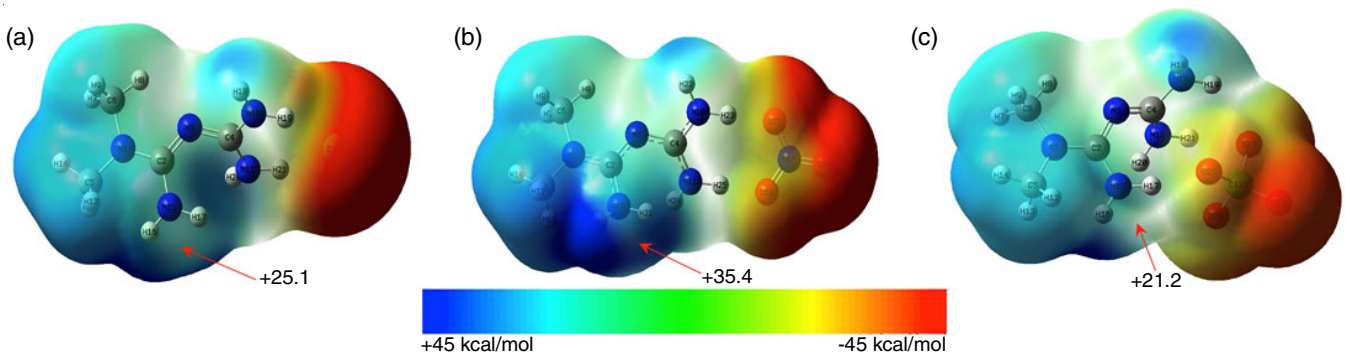

Fig. 8. Molecular electrostatic potential of (a) $MetH^+ \cdot Cl^-$, (b) $MetH^+ \cdot NO_3^-$ and (c) $MetH^+ \cdot ClO_4^-$ at rwb97xd/6-31+g(d,p) level

TABLE-7
CALCULATED HOMO AND LUMO ENERGIES (eV), BAND GAP ENERGIES (E_g, eV) AND MOLECULAR DESCRIPTORS OF METFORMIN WITH DIFFERENT COUNTER IONS

	E_{HOMO}	E_{LUMO}	E_g	η	μ	χ	ω	S
$MetH^+ \cdot Cl^-$	–1.62	0.76	2.38	1.1905	–0.430	0.430	0.110	0.420
$MetH^+ \cdot NO_3^-$	–2.14	0.73	2.87	1.435	–0.705	0.705	0.357	0.348
$MetH^+ \cdot ClO_4^-$	–3.49	0.74	4.23	2.115	–1.375	1.380	2.00	0.236

TABLE-6
CALCULATED ATOMIC CHARGES AND DIPOLE MOMENT ON METFORMIN WITH DIFFERENT COUNTER IONS

	Hirshfeld	Mullikan	D
$MetH^+ \cdot Cl^-$	0.521	0.403	5.70
$MetH^+ \cdot NO_3^-$	0.601	0.802	6.22
$MetH^+ \cdot ClO_4^-$	0.669	0.811	4.64

However, in the case of $MetH^+ \cdot ClO_4^-$, it shows higher stability. The softness is an important property that evaluates the ability of the charge transfer and is the reciprocal of the hardness. Table-7 shows that $MetH^+ \cdot Cl^-$ is the softest compound, which indicates the less stability and more reactivity. The chemical potential of the molecules are negative that indicates the molecules stability with higher values for $MetH^+ \cdot ClO_4^-$. The electrophilicity index (ω) is a good descriptor, which determines the reactivity of the molecules. Molecules with $\omega < 0.8$ eV is a weak electrophiles, $0.8 < \omega < 1.5$ eV is medium electrophiles, where the strong electrophile has $\omega > 1.5$ eV [38]. The calculated ω values shows that $MetH^+ \cdot ClO_4^-$ is strong electrophile, where $MetH^+ \cdot Cl^-$ and $MetH^+ \cdot NO_3^-$ are weak electrophiles.

Conclusion

A new crystal structure of $MetH^+ \cdot ClO_4^-$ was synthesized and characterized by different spectroscopic techniques. The obtained $MetH^+ \cdot ClO_4^-$ was protonated at the centrosymmetric N2 atom, however, the structure in solution was in equilibrium with the terminal protonated isomer. Its structure was stabilized through hexagonal hydrogen bonding network. It has been clearly demonstrated that the sites of interaction of metformin salts with ClO_4^-, Cl^- and NO_3^- can be predicted by using DFT-based reactivity descriptors such as the hardness, softness and electrophilicity, as well as Hirshfeld and Mullikan atomic charges calculations. These descriptors were used in the characterization and successfully description of the preferred reactive sites and provide a firm explanation for the reactivity of these salts. Present investigations also indicated that the positive charge on the metformin salts are increasing in the order $MetH^+ \cdot Cl^- < MetH^+ \cdot NO_3^- < MetH^+ \cdot ClO_4^-$. The dipole moment could totally change the stability behaviour of the system. Consequently, the exchange of the counter anion within the molecule causing the change of dipole moment orientation might be crucial for controlling the intermolecular interactions.

Supplementary information: Crystallographic data for the structural analysis of metformin perchlorate ($MetH^+ \cdot ClO_4^-$) has been deposited with the Cambridge Crystallographic Data Centre bearing the CCDC No. 1483522. Copies of this information are available on request free of charge from CCDC, Union Road, Cambridge, CB21EZ, U.K. (fax: +44-1223-336-033; e-mail: deposit@ccdc.ac.uk or http://www.ccdc.cam.ac.uk).

ACKNOWLEDGEMENTS

This research was funded by the University of Taif, Saudi Arabia, Deanship of Scientific Research, project No. 1-439-6069.

CONFLICT OF INTEREST

The authors declare that there is no conflict of interests regarding the publication of this article.

REFERENCES

1. D. Sweeney, M.L. Raymer and T.D. Lockwood, *Biochem. Pharmacol.*, **66**, 663 (2003); https://doi.org/10.1016/S0006-2952(03)00338-1
2. S. Villamizar-Delgado, L.M. Porras-Osorio, O. Piñeros, J. Ellena, N. Balcazar, R.E. Varela-Miranda and R.F. D'Vries, *RSC Adv.*, **10**, 22856 (2020); https://doi.org/10.1039/D0RA04059B
3. J. Li, W. Zhong, K. Zhang, D. Wang, J. Hu and M.B. Chan-Park, *ACS Appl. Mater. Interfaces*, **12**, 21231 (2020); https://doi.org/10.1021/acsami.9b17747
4. M.-D. Serb, I. Kalf and U. Englert, *CrystEngComm*, **16**, 10631 (2014); https://doi.org/10.1039/C4CE01643B
5. S. Chong-Canto, E.V. García-Báez, F.J. Martínez-Martínez, A.A. Ramos-Organillo and I.I. Padilla-Martínez, *Pharmaceutics*, **12**, 998 (2020); https://doi.org/10.3390/pharmaceutics12100998

6. K. Kaabi, K. Klai, E. Wenger, C. Jelsch, F. Lefebvre and C.B. Nasr, *Acta Crystallogr. C*, **76**, 572 (2020); https://doi.org/10.1107/S2053229620006336
7. S. Safe, V. Nair and K. Karki, *Biol. Chem.*, **399**, 321 (2018); https://doi.org/10.1515/hsz-2017-0271
8. G. Blandino, M. Valerio, M. Cioce, F. Mori, L. Casadei, C. Pulito, A. Sacconi, F. Biagioni, G. Cortese, S. Galanti, C. Manetti, G. Citro, P. Muti and S. Strano, *Nat. Commun.*, **3**, 865 (2012); https://doi.org/10.1038/ncomms1859
9. S. Bahrambeigi and V. Shafiei-Irannejad, *Biochem. Pharmacol.*, **174**, 113787 (2020); https://doi.org/10.1016/j.bcp.2019.113787
10. B. Zhao, J. Luo, T. Yu, L. Zhou, H. Lv and P. Shang, *Life Sci.*, **254**, 117717 (2020); https://doi.org/10.1016/j.lfs.2020.117717
11. T. Pappa and M. Alevizaki, *Eur. Thyroid J.*, **2**, 22 (2013); https://doi.org/10.1159/000346248
12. C. Anil, A. Kut, B. Atesagaoglu, A. Nar, N. Bascil Tutuncu and A. Gursoy, *Med. Princ. Pract.*, **25**, 233 (2016); https://doi.org/10.1159/000442821
13. X. Hu, Y. Liu, C. Wang, L. Hou, X. Zheng, Y. Xu, L. Ding and S. Pang, *Oncotarget*, **8**, 107589 (2017); https://doi.org/10.18632/oncotarget.22536
14. T.A. Altalhi, M.M. Ibrahim, A.A. Gobouri and H.S. El-Sheshtawy, *J. Mol. Liq.*, **313**, 113590 (2020); https://doi.org/10.1016/j.molliq.2020.113590
15. M. Fridrichova, I. Cisarova and I. Nemec, *Acta Crystallogr. Sect. E Struct. Rep. Online*, **68**, o18 (2012); https://doi.org/10.1107/S1600536811051105
16. M. Zhu, L. Lu and P. Yang, *Acta Crystallogr. Sect. E Struct. Rep. Online*, **59**, o586 (2003); https://doi.org/10.1107/S1600536803006639
17. M. Hariharan, S.S. Rajan and R. Srinivasan, *Acta Crystallogr. C*, **45**, 911 (1989); https://doi.org/10.1107/S0108270188014246
18. S.L. Childs, L.J. Chyall, J.T. Dunlap, D.A. Coates, B.C. Stahly and G.P. Stahly, *Cryst. Growth Des.*, **4**, 441 (2004); https://doi.org/10.1021/cg034243p
19. L. Lu, H. Zhang, S. Feng and M. Zhu, *Acta Crystallogr. Sect. E Struct. Rep. Online*, **60**, o640 (2004); https://doi.org/10.1107/S160053680400652X
20. R. Olar, M. Badea, D. Marinescu, C.-M. Chifiriuc, C. Bleotu, M.N. Grecu, E.E. Iorgulescu, M. Bucur, V. Lazar and A. Finaru, *Eur. J. Med. Chem.*, **45**, 2868 (2010); https://doi.org/10.1016/j.ejmech.2010.03.009
21. X. Huang, Y. Li, P. Wang and L. Wang, *Anal. Sci.: X-ray Structure Analysis Online*, **24**, 1563 (2008); https://doi.org/10.2116/analsci.24.1563
22. J. Dong, B. Liu and B. Yang, *Acta Crys. E*, **71**, o747 (2015); https://doi.org/10.1107/S2056989015016771
23. R. Olar, M. Badea, D. Marinescu, M. Chifiriuc, C. Bleotu, M.N. Grecu, E. Iorgulescu and V. Lazar, *Eur. J. Med. Chem.*, **45**, 3027 (2010); https://doi.org/10.1016/j.ejmech.2010.03.033
24. D. Kathuria, A.A. Bankar and P.V. Bharatam, *J. Mol. Struct.*, **1152**, 61 (2018); https://doi.org/10.1016/j.molstruc.2017.08.100
25. K. Koperwas, K. Adrjanowicz, A. Grzybowski and M. Paluch, *Sci. Rep.*, **10**, 283 (2020); https://doi.org/10.1038/s41598-019-57158-4
26. G.M. Sheldrick, SADABS, Area-Detector Absorption Correction, Göttingen, Germany (1996).
27. SAINTPlus Data Reduction and Correction Program, v. 6.45a; Bruker AXS: Madison, WI (2003).
28. G.M. Sheldrick, SHELXL1997, University of Göttingen, Germany (1997).
29. M.J. Frisch, G.W. Trucks, H.B. Schlegel, G.E. Scuseria, M.A. Robb, J.R. Cheeseman, G. Scalmani, V. Barone, G.A. Petersson, H. Nakatsuji, X. Li, M. Caricato, A.V. Marenich, J. Bloino, B.G. Janesko, R. Gomperts, B. Mennucci, H.P. Hratchian, J.V. Ortiz, A.F. Izmaylov, J.L. Sonnenberg, D. Williams-Young, F. Ding, F. Lipparini, F. Egidi, J. Goings, B. Peng, A. Petrone, T. Henderson, D. Ranasinghe, V.G. Zakrzewski, J. Gao, N. Rega, G. Zheng, W. Liang, M. Hada, M. Ehara, K. Toyota, R. Fukuda, J. Hasegawa, M. Ishida, T. Nakajima, Y. Honda, O. Kitao, H. Nakai, T. Vreven, K. Throssell, J. A. Montgomery, Jr., J.E. Peralta, F. Ogliaro, M.J. Bearpark, J.J. Heyd, E.N. Brothers, K.N. Kudin, V.N. Staroverov, T.A. Keith, R. Kobayashi, J. Normand, K. Raghavachari, A.P. Rendell, J.C. Burant, S.S. Iyengar, J. Tomasi, M. Cossi, J.M. Millam, M. Klene, C. Adamo, R. Cammi, J.W. Ochterski, R.L. Martin, K. Morokuma, O. Farkas, J.B. Foresman and D.J. Fox, Gaussian, Inc., Wallingford CT, Gaussian 16, Revision C.01 (2016).
30. C. Herrnstadt, D. Mootz, H. Wunderlich and H. Möhrle, *J. Chem. Soc., Perkin Trans. II*, 735 (1979); https://doi.org/10.1039/P29790000735
31. S.C. Jagdale, S.A. Patil, B.S. Kuchekar and A.R. Chabukswar, *J. Young Pharm.*, **3**, 197 (2011); https://doi.org/10.4103/0975-1483.83758
32. S. Ramukutty, R. Jeyasudha and E. Ramachandran, *Res. Rev. J. Pharm. Pharm. Sci.*, **3**, 36 (2014).
33. R.C. Hirt and R.G. Schmitt, *Spectrochim. Acta*, **12**, 127 (1958); https://doi.org/10.1016/0371-1951(58)80025-9
34. W. Sun, G. Yuan, J. Liu, L. Ma and C. Liu, *Spectrochim. Acta A Mol. Biomol. Spectrosc.*, **106**, 275 (2013); https://doi.org/10.1016/j.saa.2012.12.090
35. H.S. El-Sheshtawy and A.M. Abou Baker, *J. Mol. Struct.*, **1067**, 225 (2014); https://doi.org/10.1016/j.molstruc.2014.03.042
36. S. Gunasekaran, R.A. Balaji, S. Kumaresan, G. Anand and S. Srinivasan, *Can. J. Anal. Sci. Spectrosc.*, **53**, 149 (2008).
37. R.G. Pearson, *J. Chem. Sci.*, **117**, 369 (2005); https://doi.org/10.1007/BF02708340
38. L.R. Domingo, M.J. Aurell, P. Pérez and R. Contreras, *Tetrahedron*, **58**, 4417 (2002); https://doi.org/10.1016/S0040-4020(02)00410-6